Modeling extracellular fields for a three-dimensional network of cells using NEURON

Appukuttan, Shailesh; Brain, Keith L; Manchanda, Rohit

DOI:
10.1016/j.jneumeth.2017.07.005
10.1016/j.jneumeth.2017.07.005

Document Version
Peer reviewed version

Citation for published version (Harvard):
Appukuttan, S, Brain, KL & Manchanda, R 2017, 'Modeling extracellular fields for a three-dimensional network of cells using NEURON', *Journal of Neuroscience Methods*, vol. 290, NSM_7781, pp. 27-38. https://doi.org/10.1016/j.jneumeth.2017.07.005, https://doi.org/10.1016/j.jneumeth.2017.07.005

Modeling Extracellular Fields for a Three-Dimensional Network of Cells using NEURON

Shailesh Appukuttan[1,*], Keith L. Brain[2], Rohit Manchanda[1]

[1] *Department of Biosciences and Bioengineering, Indian Institute of Technology Bombay, Mumbai, Maharashtra, India*

[2] *School of Clinical and Experimental Medicine, College of Medical and Dental Sciences, University of Birmingham, Birmingham, UK*

Abstract

Background: Computational modeling of biological cells usually ignores their extracellular fields, assuming them to be inconsequential. Though such an assumption might be justified in certain cases, it is debatable for networks of tightly packed cells, such as in the central nervous system and the syncytial tissues of cardiac and smooth muscle.

New Method: In the present work, we demonstrate a technique to couple the extracellular fields of individual cells within the NEURON simulation environment. The existing features of the simulator are extended by explicitly defining current balance equations, resulting in the coupling of the extracellular fields of adjacent cells.

Results: With this technique, we achieved continuity of extracellular space for a network model, thereby allowing the exploration of extracellular interactions computationally. Using a three-dimensional network model, passive and active electrical properties were evaluated under varying levels of extracellular volumes. Simultaneous intracellular and extracellular recordings for synaptic and action potentials were analyzed, and the potential of ephaptic transmission towards functional coupling of cells was explored.

*Current Address: *Neuroinformatics group, Unité de Neurosciences, Information et Complexité, Centre National de la Recherche Scientifique, Gif sur Yvette, France*

Comparison with Existing Method(s): We have implemented a true bi-domain representation of a network of cells, with the extracellular domain being continuous throughout the entire model. This has hitherto not been achieved using NEURON, or other compartmental modeling platforms.

Conclusions: We have demonstrated the coupling of the extracellular field of every cell in a three-dimensional model to obtain a continuous uniform extracellular space. This technique provides a framework for the investigation of interactions in tightly packed networks of cells via their extracellular fields.

Keywords: Extracellular Space, Electrical Syncytium, Compartmental Modeling, NEURON, Extracellular Recordings, Triphasic Action Potential, Ephaptic Coupling

1. Introduction

Electrical modeling techniques for biological cells, such as the compartmental approach (Rall, 1964), involve the conversion of cellular features into their electrical equivalents. Cells and networks are described in terms of combinations of various electrical components, forming large complex circuits. Compartmental modeling platforms, such as NEURON, simulate these models by solving the resultant electrical equivalent circuits (Hines & Carnevale, 1997). When undertaking such modeling, it is common practice to ignore the extracellular fields, assuming them to be inconsequential in determining transmembrane voltage changes (Rall, 1959; Koch, 2004). All points outside the membrane are considered to be connected to ground. This might be a reasonable assumption in cases where the interstitial space between cells is large, resulting in a low value of extracellular resistance. This allows for considerable simplification in the

electrical equivalent circuit, and its analysis. But for tissues where cells are tightly packed together, such as in the central nervous system and the syncytial tissues of cardiac and smooth muscle, this assumption might not be justified. Here, the peripheral cells might have a relatively large volume of extracellular space around them, but the bulk of the cells that lie in the interior and are closely packed, may be surrounded by very little interstitial space. For such cells, the resistance offered by the extracellular field could be significant and is likely to influence their electrical activity. Goldwyn & Rinzel (2016) demonstrated that a neuronal population could generate millivolt-scale extracellular potentials, and that this could induce millivolt-scale perturbations in the membrane potential of a neuron. As the cells are part of an electrical network, the effects will not remain localized but propagate to a more macroscopic level, and may affect tissue function. For example, it has been reported that differences in the extracellular resistance between the peripheral cells and those in the interior, affects the shape of the excitation wavefront with the former leading action potential propagation (Suenson, 1991).

Reduced extracellular volume also brings about the possibility of ephaptic coupling, whereby electrical transmission between adjacent cells is feasible even in the absence of intercellular pathways, by means of electric field interactions between them (Holt & Koch, 1999; Mori et al., 2008). It has been shown that action potential propagation could occur even in the absence of functional gap junctions (Sperelakis & McConnell, 2002). Such coupling could arise not just at junctional clefts between cells, but also at other regions where the cells are in close proximity (Lin & Keener, 2013). The phenomenon of ephaptic transmission holds significance especially for: (i) nerve fibers in the central nervous system where many axons are unmyelinated and densely packed, such as in the

olfactory system, and (ii) syncytial tissues, such as cardiac and smooth muscle, owing to their tight packing of cells. It has been argued that coupling between cells in syncytial tissues exists not merely owing to the presence of gap junctions, but also as an outcome of electric field interactions, with the latter playing a more dominant role in certain scenarios (Lin & Keener, 2013), particularly over regions of the cells where gap junctions are not present. Impulse transmission by means of ephaptic coupling has been demonstrated to be feasible between two intestinal smooth muscle bundles (Sperelakis & McConnell, 2002). Though the functional role of ephaptic coupling has been widely argued (Sperelakis, 2002), there has been a dearth of any focused computational studies towards its investigation (Koch, 2004).

There exist cable theory formalisms that account for extracellular space (Plonsey & Barr, 1991; Bédard & Destexhe, 2013), thereby enabling quantitative predictions. But traditional cable theory and its derivatives are applicable only for uniform continuous cable structures. In the present work, we model individual cells as small cable segments. These are coupled to each other by means of discrete gap junctional coupling mechanisms to form a long one-dimensional chain, and subsequently extended to form a three-dimensional network. Keener (1990, 1991) has demonstrated that the traditional cable theory cannot be applied to such structures, and proposes a modified cable theory to incorporate the effect of discrete gap junctions. Unfortunately, this modified cable theory does not consider the extracellular space as it is derived under the assumption of an extensive extracellular medium.

The work presented here describes a technique to explore extracellular interactions computationally by enabling continuity of extracellular space for a network model. The implementation is presented for the NEURON simulation platform, a widely employed

tool for modeling neurons and neuronal networks (Hines & Carnevale, 1997). It has also been employed for modeling cardiac (Casaleggio et al., 2014) and smooth muscle tissue (Appukuttan et al., 2015a). NEURON employs the compartmental modeling approach and supports features for implementing extracellular fields. For example, a neuronal model comprising soma, axon and dendrites can be developed, and NEURON would automatically connect the extracellular fields of the various sections. A limitation is that the extracellular fields of individual cells are not coupled in the same manner. Thus, when attempting to model a network of cells, such as a cardiac syncytium or a bundle of smooth muscle cells, or closely packed never fibers, the extracellular field of each cell is disconnected from that of other cells in its neighborhood. Naturally, this does not offer an accurate representation of interstitial space in the tissue, and would also disallow the investigation of ephaptic coupling.

We here demonstrate a technique to couple the extracellular fields of individual cells within the NEURON environment, so as to obtain a continuous extracellular space. We extend this technique to connect the extracellular fields of all cells in an electrical network. A model of the detrusor syncytium has been adopted for this purpose (Appukuttan et al., 2015a). This model provides the benefit of reduced cellular morphology, uniformity in arrangement of cells within the network, and an opportunity to compare and contrast electrical response owing to gap junctional and ephaptic coupling. This affords a simpler demonstration of the implementation and its analysis, but the approach presented can be extended to any configuration of electrical networks of cells. The extracellular fields of peripheral and internal cells have been differentiated in our study to reflect the differences in volume of extracellular space around the cells. Certain predictions regarding electrical transmission and action potential (AP)

propagation were tested using the model developed, and the potential effect of ephaptic coupling was explored. Finally, to demonstrate the ease of extending this technique towards neuronal networks, we present an example of implementing this method for coupling the extracellular fields of two adjacent neurons and present certain outcomes from their simulation.

2. Methods

Fig. 1 illustrates the electrical equivalent circuit for a cell, modeled as a cylinder with three segments, without an explicit extracellular field. The cell is endowed with passive membrane channels. Each compartment consists of a parallel combination of a resistor and a capacitor (R-C), with the former representing the conductivity of the passive ion channels (g_pas) and the latter representing the capacitance due to the lipid bilayer of

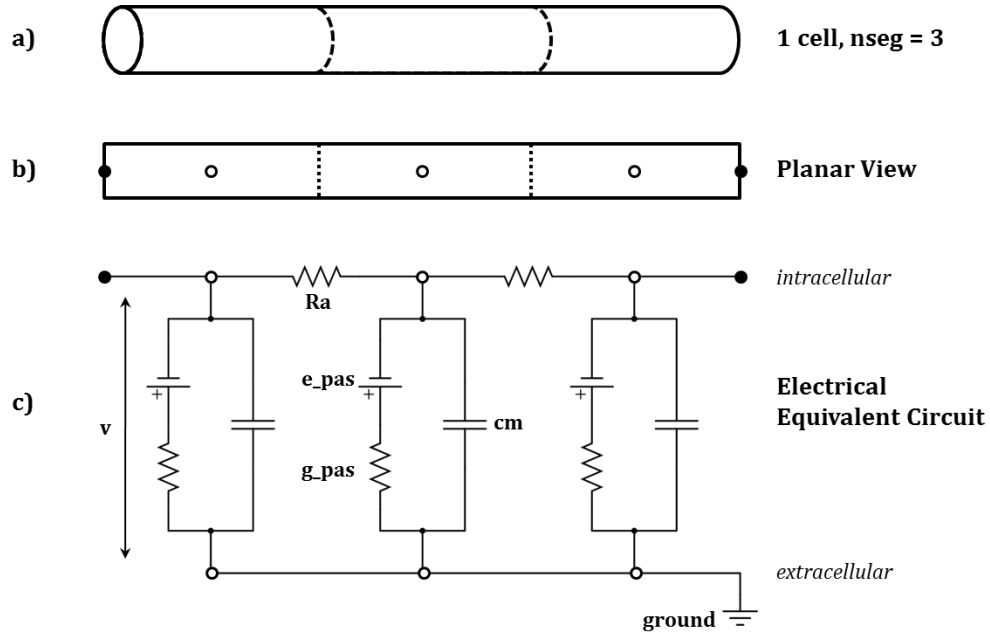

Figure 1: Illustration of a single cell in NEURON (a) Conceptual model, (b) Planar view of model showing division into three compartments, (c) electrical equivalent circuit of cell. Internal and terminal nodes are marked using hollow and filled circles, respectively. Parameters have been named in accordance with the NEURON simulator, with their values tabulated in Table 2.

the cell membrane (cm). The voltage source in series with the resistance represents the reversal potential of the passive channels (e_pas). The compartments are connected intracellularly via resistive pathways denoting the cytoplasmic resistivity (Ra), while extracellularly all are connected to ground. Each compartment is represented via an internal node (hollow circles), while the extremities of the cell (or section) are represented by terminal nodes (filled circles). The membrane potential (v) for each compartment is measured across its R-C circuit (as shown in Fig. 1), i.e. the difference of the intracellular potential (v_i) and the extracellular potential (v_e) (Eq. 1). The latter is equal to zero when the extracellular space is grounded, and the membrane potential equates to the internal potential.

$$v = v_i - v_e \tag{1}$$

The extracellular field can be incorporated into cells in NEURON using the built-in *extracellular* mechanism. By default, it equips each section with two layers of extracellular field, but can be changed if desired. With the incorporation of the *extracellular* mechanism to the above model, we obtain two layers of extracellular field for each compartment. Every compartment will now have an internal node, and two extracellular nodes, vext[0] & vext[1]. This is illustrated in Fig. 2.

Each layer has an R-C circuit, produced by the parallel combination of xg and xc, with the last layer additionally having a voltage source in series with the resistor. The extracellular potential (v_e) just outside the membrane is termed vext[0] in NEURON, and is no longer directly connected to ground. Hence, v_e can now influence the membrane potential (v). The internal potential (v_i), when required, can be evaluated as the sum of v and v_e. The extracellular layers of adjacent compartments are connected by means of axial resistances (xraxial).

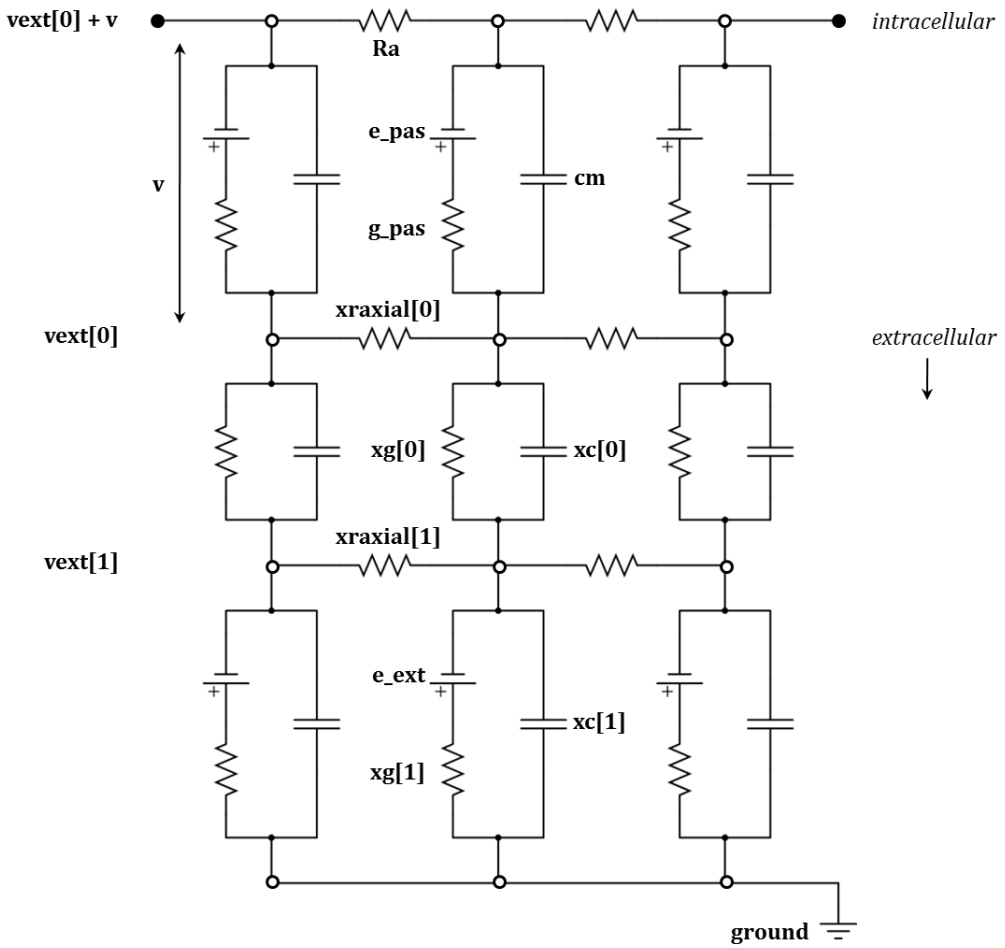

Figure 2: Electrical equivalent circuit of a cell, divided into three compartments, in NEURON with the default extracellular mechanism. Parameters have been named in accordance with the NEURON simulator, with their values tabulated in Tables 1 and 2. Note the presence of two layers of extracellular field.

NEURON offers these multi-layer representations of the extracellular space to enable modeling of various biophysical and/or experimental settings. For example, the resistive components in the membrane-adjacent layer allows for inclusion of nearest-neighbor extracellular interactions, such as mimicking an unmyelinated axon surrounded by a thin layer of extracellular electrolyte, suspended in an oil bath. The capacitive components in this layer allow for simplistic representation of myelination. The outermost layer, containing the voltage source, is useful mostly as a hook for applying an extracellular driving force to the cell. But all these parameters can be utilized in other ways as per the modeling requirements.

Table 1: Parameters provided by extracellular mechanism, with their units and values. The parameter names and units have been kept consistent with the NEURON simulator, and correspond to those in Fig. 2. NEURON requires values of axial resistors to be specified as resistivities and those of radial resistors as conductivities. Infinity has been specified as 10^9 and zero represented by 10^{-9}. The latter was found necessary to eliminate certain errors in numerical integration. Note that xg[0] has different values for peripheral and internal cells in a syncytium.

Parameter	Units	Value
xraxial[0]	MΩ/cm	161.8
xc[0]	μF/cm^2	0
xg[0]	S/cm^2	10^9 / 10^{-9}
xraxial[1]	MΩ/cm	10^9
xc[1]	μF/cm^2	0
xg[1]	S/cm^2	10^9
e_ext	mV	0

As the objective of the current study is to demonstrate the linking of extracellular fields of individual cells, it is useful to reduce the extracellular field to a single layer. The same methodology can then be followed for other layers, where required. Simplifying the extracellular field can be achieved by adjusting the parameters of the *extracellular* mechanism. The various parameters, their dimensions, and their values for the simplified model are listed in Table 1. By setting the parameters of the second extracellular layer (xraxial[1], xc[1], xg[1], e_ext) as specified in Table1, we are able to connect the first layer directly to ground. Additionally, setting the capacitance of the first extracellular layer (xc[0]) to zero, allows us to obtain a purely resistive extracellular field. This is a common representation that is undertaken when modeling extracellular spaces (Bennett et al., 1993; Lindén et al., 2013). The combined effect of the above is illustrated in Fig. 3, where the cell has a single resistive extracellular layer.

Determination of values for the remaining parameters (xraxial[0] and xg[0]) is discussed in section 2.3.

2.1. Coupling Extracellular Fields

When we create two individual cells in NEURON, with the aforementioned specifications, each of them will have an electrical equivalent circuit as shown in Fig. 3. They will be electrically isolated from one another, both intracellularly and extracellularly. The cells can be linked intracellularly by means of gap junctions and several such modeling studies have been carried out in the past (Crane et al., 2001; Migliore et al., 2005). Gap junctions are often modeled as passive resistive pathways linking two cells. Setting up intracellular coupling in NEURON is relatively simple, and we have in the past extended this approach to simulate large 3-D networks of smooth muscle cells (Appukuttan et al., 2015a). The problem addressed in the present study is the linking of the extracellular fields of two cells.

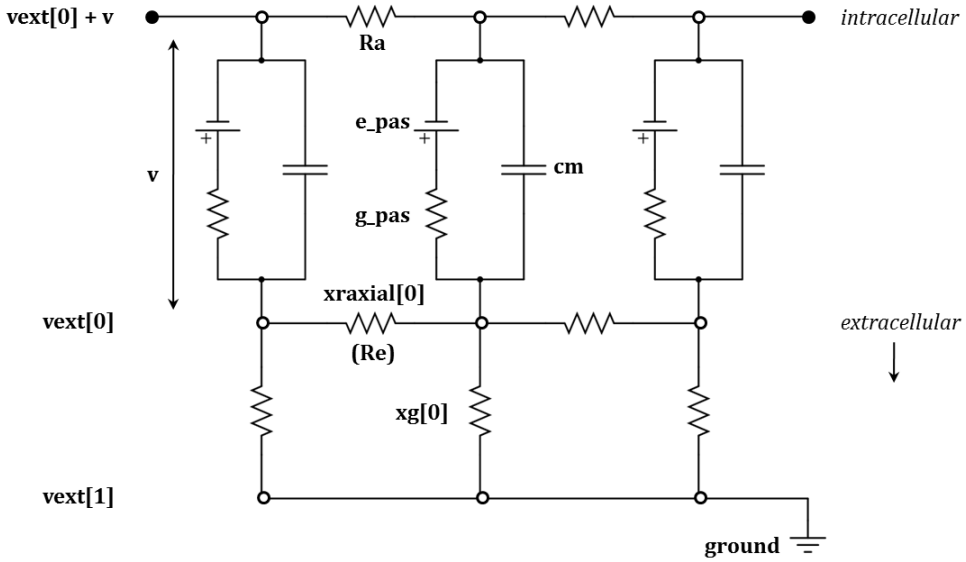

Figure 3: Electrical equivalent circuit of a cell, divided into three compartments, in NEURON with simplified extracellular mechanism. The modified model has only a single layer of extracellular field.

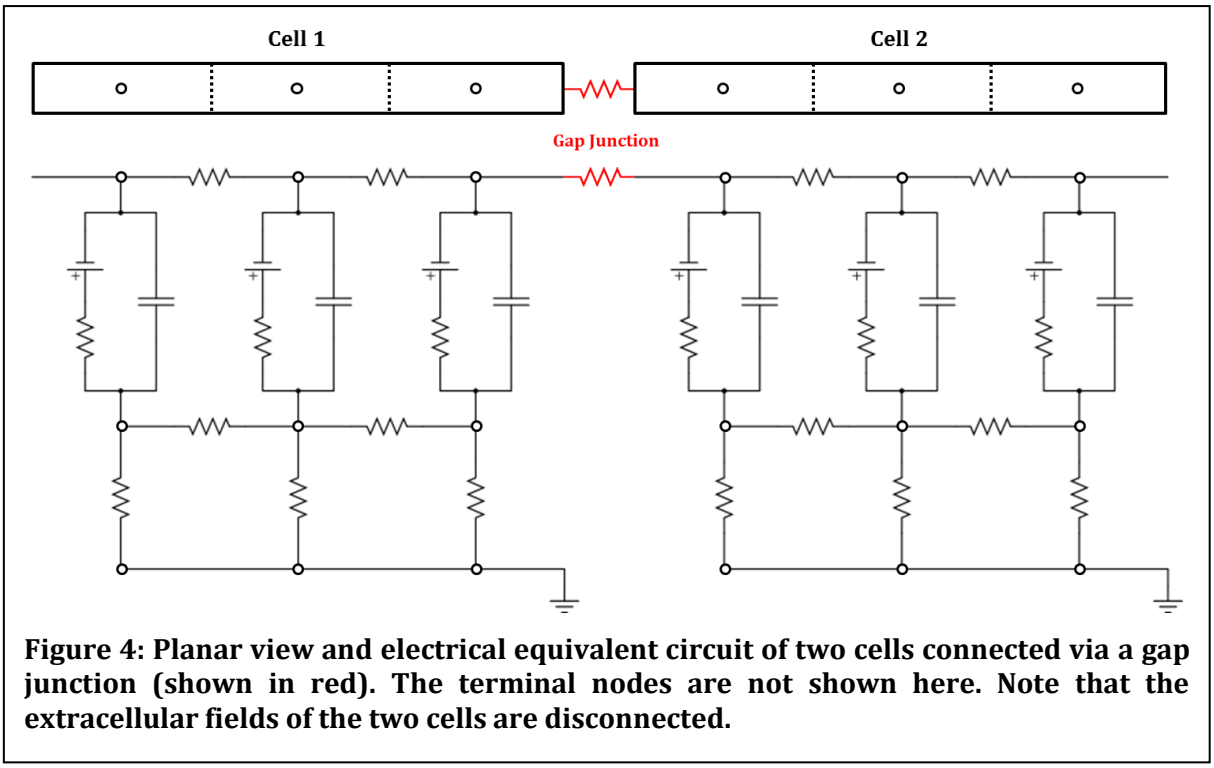

Figure 4: Planar view and electrical equivalent circuit of two cells connected via a gap junction (shown in red). The terminal nodes are not shown here. Note that the extracellular fields of the two cells are disconnected.

For purposes of exposition, consider a model of two identical cells, each having a single resistive layer of extracellular field, and coupled end-to-end electrically by means of gap junctions, as presented in Fig. 4. As seen in the figure, the extracellular fields of the two cells are still not directly connected, and thus extracellular potentials of cell 1 cannot directly affect those of cell 2. Any effect will be indirect owing to the gap junctional coupling of the intracellular regions. This would clearly not be a faithful representation of the topology that obtains physiologically, where the extracellular space does not feature such discontinuities. To overcome this mismatch, we require an 'extracellular link' between the adjacent extracellular nodes of the two cells, as illustrated in Fig. 5. It should be noted that though this connection appears similar to the gap junctional resistance that couples the internal nodes of adjacent cells, NEURON does not allow the same approach for modeling links between extracellular nodes. The solution lies in explicitly defining current balance equations to be solved by NEURON. This can be accomplished using the *LinearMechanism* class offered by NEURON. The relevant current balance equations that need to be defined are:

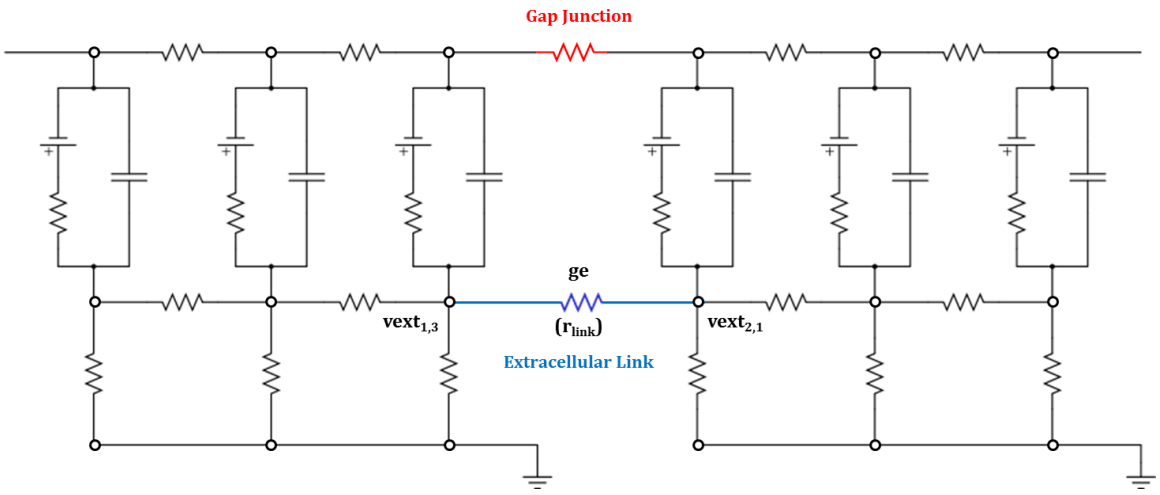

Figure 5: Electrical equivalent circuit of two cells connected via gap junction (shown in red) with coupled extracellular mechanisms (shown in blue). The terminal nodes are not shown here.

$$I_{ext_{1\to2}} = -I_{ext_{2\to1}} \tag{2}$$

$$I_{ext_{1\to2}} = ge\times\{vext_{1,3} - vext_{2,1}\} \tag{3}$$

$$I_{ext_{2\to1}} = ge\times\{vext_{2,1} - vext_{1,3}\} \tag{4}$$

Expanding the terms, we get,

$$I_{ext_{1\to2}} = (ge\times vext_{1,3}) - (ge\times vext_{2,1}) \tag{5}$$

$$I_{ext_{2\to1}} = -(ge\times vext_{1,3}) + (ge\times vext_{2,1}) \tag{6}$$

where ge is the conductance of the extracellular link, $vext_{1,3}$ and $vext_{2,1}$ are the extracellular potentials (v_e) at the 3rd node of cell 1 and 1st node of cell 2, respectively (see Fig. 5), and $I_{ext_{1\to2}}$ and $I_{ext_{2\to1}}$ are the currents flowing across the extracellular link from cell 1 to 2, and cell 2 to 1, respectively. These equations are fed into NEURON by means of the *LinearMechanism* class as presented in the following section.

It should be noted that the extracellular link can be established even in the absence of gap junctional coupling. Such a configuration is discussed in section 3.1, and also in section 3.4 while evaluating ephaptic coupling. Here, we have presented both gap

junctional coupling and the extracellular link to help illustrate the difference in the underlying electrical equivalent circuits.

2.2 Implementing Extracellular Link Using LinearMechanism

The template equation for *LinearMechanism* is given by:

$$c\frac{dy}{dt} + gy = b \tag{7}$$

As the extracellular link to be modeled does not have a capacitive component (c), Eq. 7 reduces to:

$$gy = b \tag{8}$$

Eqs. 5 and 6 can be fitted into this form by having:

$$g = \begin{bmatrix} ge & -ge \\ -ge & ge \end{bmatrix}, \quad y = \begin{bmatrix} vext_{1,3} \\ vext_{2,1} \end{bmatrix}, \quad b = \begin{bmatrix} 0 \\ 0 \end{bmatrix} \tag{9}$$

The specific compartments that are to be linked extracellularly, e.g. the last compartment of cell 1 with the first compartment of cell 2, are defined by means of the other input parameters of the *LinearMechanism* class, namely *sl* and *xvec*. The optional parameter *[layervec]* allows specification of the extracellular layer in context. The above approach can be extended to couple the extracellular space of a chain of several cells. Fig. 6 shows examples of a chain of three cells, coupled longitudinally and transversely. The gap junctions are not shown in the figure for simplicity. For longitudinal coupling, the gap junctions can be connected end-to-end (see Fig. 4), whereas for transverse coupling, they can be modeled as linked across the entire length of the cells, or merely across the central compartments. We prefer the latter approach, in accordance with our past studies (Appukuttan et al., 2015a). In terms of the extracellular fields, a major difference between longitudinal and transverse configurations lies in the number of extracellular links that are required to be established. In the case of longitudinal

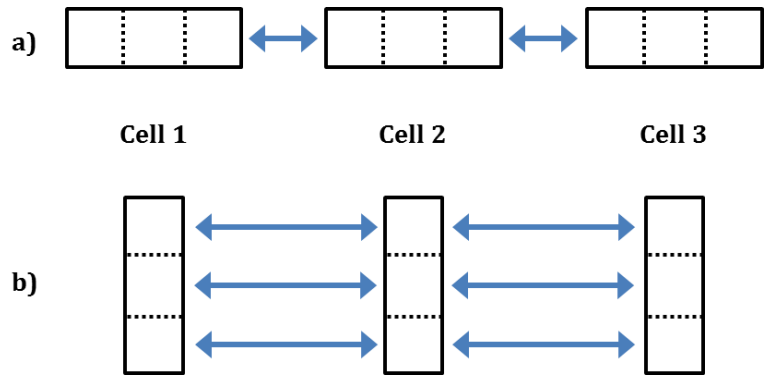

Figure 6: Chain of three cells electrically coupled (a) longitudinally, (b) transversely. For simplicity gap junctions are not shown, and only extracellular links between the cells are illustrated (represented by arrows). It should be noted that the extracellular links, irrespective of the orientation of coupling, are always established via *ge*.

coupling, only the most adjacent compartments between cells need to be linked extracellularly (Fig. 6a), while under transverse coupling, each of the corresponding compartments of adjacent cells need to be linked extracellularly (Fig. 6b). The parameters in Eq. 9 would be specified as shown in Eqs. 10 and 11 for the longitudinal and transverse coupling examples, respectively, discussed here. Certain elements of parameter g for the transverse configuration have double the conductance value owing to the corresponding nodes ($vext_{2,1}$, $vext_{2,2}$, $vext_{2,3}$) forming two extracellular links, one each with cells 1 and 3.

$$g = \begin{bmatrix} ge & -ge & 0 & 0 \\ -ge & ge & 0 & 0 \\ 0 & 0 & ge & -ge \\ 0 & 0 & -ge & ge \end{bmatrix}, \quad y = \begin{bmatrix} vext_{1,3} \\ vext_{2,1} \\ vext_{2,3} \\ vext_{3,1} \end{bmatrix}, \quad b = \begin{bmatrix} 0 \\ 0 \\ 0 \\ 0 \end{bmatrix} \tag{10}$$

$$g = \begin{bmatrix} ge & 0 & 0 & -ge & 0 & 0 & 0 & 0 & 0 \\ 0 & ge & 0 & 0 & -ge & 0 & 0 & 0 & 0 \\ 0 & 0 & ge & 0 & 0 & -ge & 0 & 0 & 0 \\ -ge & 0 & 0 & 2ge & 0 & 0 & -ge & 0 & 0 \\ 0 & -ge & 0 & 0 & 2ge & 0 & 0 & -ge & 0 \\ 0 & 0 & -ge & 0 & 0 & 2ge & 0 & 0 & -ge \\ 0 & 0 & 0 & -ge & 0 & 0 & ge & 0 & 0 \\ 0 & 0 & 0 & 0 & -ge & 0 & 0 & ge & 0 \\ 0 & 0 & 0 & 0 & 0 & -ge & 0 & 0 & ge \end{bmatrix}, \quad y = \begin{bmatrix} vext_{1,1} \\ vext_{1,2} \\ vext_{1,3} \\ vext_{2,1} \\ vext_{2,2} \\ vext_{2,3} \\ vext_{3,1} \\ vext_{3,2} \\ vext_{3,3} \end{bmatrix}, \quad b = \begin{bmatrix} 0 \\ 0 \\ 0 \\ 0 \\ 0 \\ 0 \\ 0 \\ 0 \\ 0 \end{bmatrix} \tag{11}$$

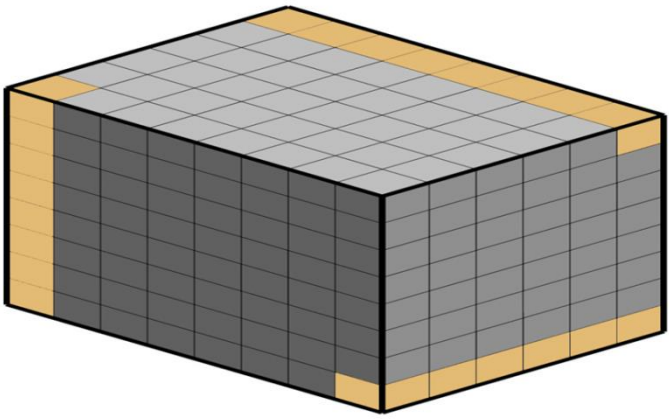

Figure 7: Representation of a 3-D syncytium of cells arranged in a cubic lattice layout. An example of a chain of cells along each of the three axes is highlighted. Each sub-block represents a single cell.

The implementations of these examples were validated via equivalent circuit representations on Multisim®, a SPICE based simulation environment developed by National Instruments, capable of checking the integrity of circuit designs and to predict their behavior. The above approach of linking extracellular spaces of chains of cells can be employed to develop three-dimensional syncytial models of cells. This can be accomplished by employing arrays of *LinearMechanism* instances, one for each of the longitudinal and transverse chains present in the network, as illustrated in Fig. 7.

2.3 Model Development and Modifications

The development of the three-dimensional model of smooth muscle cells is as described in an earlier study (Appukuttan et al., 2015a), where the cells were coupled only intracellularly by means of gap junctions. The parameters, and their values, that define the biophysical properties of individual cells are described in Table 2. In the present model we also incorporate the coupling of the extracellular fields using the approach discussed earlier. The number of compartments per cell (nseg) was reduced to 5 for the 3-D model in view of the increased complexity owing to the addition of the extracellular

Table 2: Parameters used for defining individual cells in NEURON when equipped with only passive membrane channels

Parameter	Symbol	Value
Cell Length	L	200 μm
Cell Diameter	diam	6 μm
Compartments per Cell	nseg	51 (1-D) / 5 (3-D)
Cytoplasmic Resistivity	Ra	183 Ω.cm
Membrane Resistivity	Rm	132.5 kΩ.cm^2
Membrane Capacitance	cm	1 μF/cm^2
Resting Potential	e_pas	−50 mV
Gap Junctional Resistance	–	30.6 MΩ

fields. For exploration of active membrane properties, the cells were endowed with Hodgkin-Huxley (HH) channels, enabling them to produce APs. It should be noted that this does not result in a physiologically accurate AP for the tissue under consideration, but offers a well understood paradigm for the analysis of the model. Once a physiologically relevant AP mechanism for the detrusor is satisfactorily developed, it can be easily substituted into the model. At the present time such a model is unavailable, and the focus here lies in the demonstration of the extracellular coupling and to explore its influence on the electrical activity of syncytial tissues.

An important step in setting up the extracellular field is to determine the volume of interstitial space and its resistivity. This is often defined in terms of a ratio of the intracellular to extracellular resistivities (Ra/Re) (Bennett et al., 1993; Roth, 1997). As experimental studies on the detrusor have not focused on quantifying the extracellular space, we set Ra/Re = 4 based on an earlier discrete model developed for smooth muscle (Bennett et al., 1993). As Ra in our model is 183 Ω.cm, Re evaluates to 45.75

Ω.cm, which translates to a value of 161.8 MΩ/cm for xraxial[0] (see Eq. 12; note that Re is multiplied by 1e-6 to convert units to MΩ.cm).

$$xraxial[0] = \frac{extracellular\ resitivity}{cross-sectional\ area} = \frac{Re \times 1e-6}{\pi \times (3e-4)^2} = 161.8\ M\Omega/cm \qquad (12)$$

Another factor to be considered is the differences in interstitial space between peripheral and internal cells in a syncytium. Cells on the periphery are expected to have access to a larger volume of extracellular space as compared to those located in the interior. The former can be modeled as having a direct connection to ground by setting xg[0] to infinity, while the limited extracellular space for the latter is realized by setting xg[0] to zero. The path to ground for these cells is, effectively, via their connection to the peripheral cells. The final parameter that needs to be defined is the conductance of the extracellular link (ge). In this study, we have set ge equal to the extracellular conductance between any two adjacent compartments of the cells. As Re is 47.75 Ω.cm, the absolute resistance (r_{link}) between the extracellular nodes of adjacent compartments in our model is 0.647 MΩ, and this translates to 0.205 S/cm^2 as shown in Eqs. 13 and 14. Note that in Eq. 14, r_{link} is adjusted to obtain value in Siemens, and that the surface area refers to the curved surface area of a single compartment of the cell. Such a configuration would maintain isotropy across the extracellular space of the entire syncytial model, both along the longitudinal and transverse axes.

$$r_{link} = xraxial[0] \times \frac{cell\ length}{nseg} = 161.8 \times \frac{200e-4}{5} \approx 0.647\ M\Omega \qquad (13)$$

$$g_e = \frac{1}{r_{link} \times surface\ area} = \frac{1e-6}{0.647} \times \frac{1}{2\pi \times 3e-4 \times \frac{200e-4}{5}} \approx 0.205\ S/cm^2 \qquad (14)$$

It is important to note that while modeling gap junctions in the presence of extracellular mechanism, the gap junctional current should be defined as ELECTRODE_CURRENT as

opposed to NONSPECIFIC_CURRENT. The latter is defined in NEURON as a membrane current, and would thereby result in the contribution of the gap junctional current to the transmembrane current. Ideally, gap junctional current should be considered as moving between the intracellular regions of two cells, and not being transferred via the extracellular space. Hence, it should not make any direct contribution to the transmembrane current. Also, for a NONSPECIFIC_CURRENT, v refers to the true transmembrane potential whereas for an ELECTRODE_CURRENT, v refers to the internal potential, i.e. relative to ground; the sum of transmembrane potential and any radial voltage drop across the extracellular mechanism. Gap junction mechanisms, if present, should be modified in accordance to the above.

3. Results

3.1 Demonstration of Extracellular Coupling

To demonstrate the linking of extracellular fields, we shall consider a simple model involving only two cells, such as in Fig. 4, but without gap junctional coupling between the cells. One of the cells (Cell 1) is excited at its center by means of synaptic activity, mimicked using an AlphaSynapse (Hines & Carnevale, 2001). The observed peak depolarizations at the nearest intracellular and extracellular nodes, between the two cells, is summarized in Table 3. When the extracellular fields are disconnected, the depolarization in Cell 1 is neither propagated to Cell 2, nor does it affect its extracellular field. But when we link their extracellular fields using the approach presented earlier, it is seen that the depolarization in Cell 1 causes a change in the extracellular field of Cell 2

Table 3: Peak depolarizations observed at the adjacent intracellular and extracellular nodes of two cells, in the absence and presence of the extracellular link. Cell1 is excited by means of synaptic activity.

Cell	Parameter	Without Link	With Link
Cell1	v	23.92 mV	23.92 mV
	vext[0]	2.48 μV	1.24 μV
Cell2	v	0 mV	0 mV
	vext[0]	0 μV	1.24 μV

as well. This demonstrates that we have been able to link the two extracellular spaces. It can be noted that this does not produce any change in the peak depolarization of Cell 1.

3.2 Passive and Active Electrical Properties

Various electrical parameters were evaluated using a 1-D model of a chain of 181 cells, coupled to each other intracellularly via gap junctions, and extracellularly by means of the extracellular link described earlier. These include parameters often used to describe passive membrane properties, such as the length constant, time constant, and the input resistance. The stimulus was applied at the central cell, and the total number of cells (181) was set such as to prevent reflection of current at the ends (Jack et al., 1975). The parameters were evaluated for various values of Ra/Re.

Fig. 8 plots these parameters with respect to the centrally located cell. It can be seen that all the parameters begin to settle from Ra/Re = 2 onwards. For lower ratios, representing limited interstitial volumes, there is a sharp decline in the length constant and input resistance, and a rapid rise in the time constant. With the incorporation of HH channels, the cells were capable of producing APs. This allowed the determination of AP propagation velocity. It was found that the AP propagation velocity increased with an increase in the extracellular volume, before eventually saturating at around 30 cm/s.

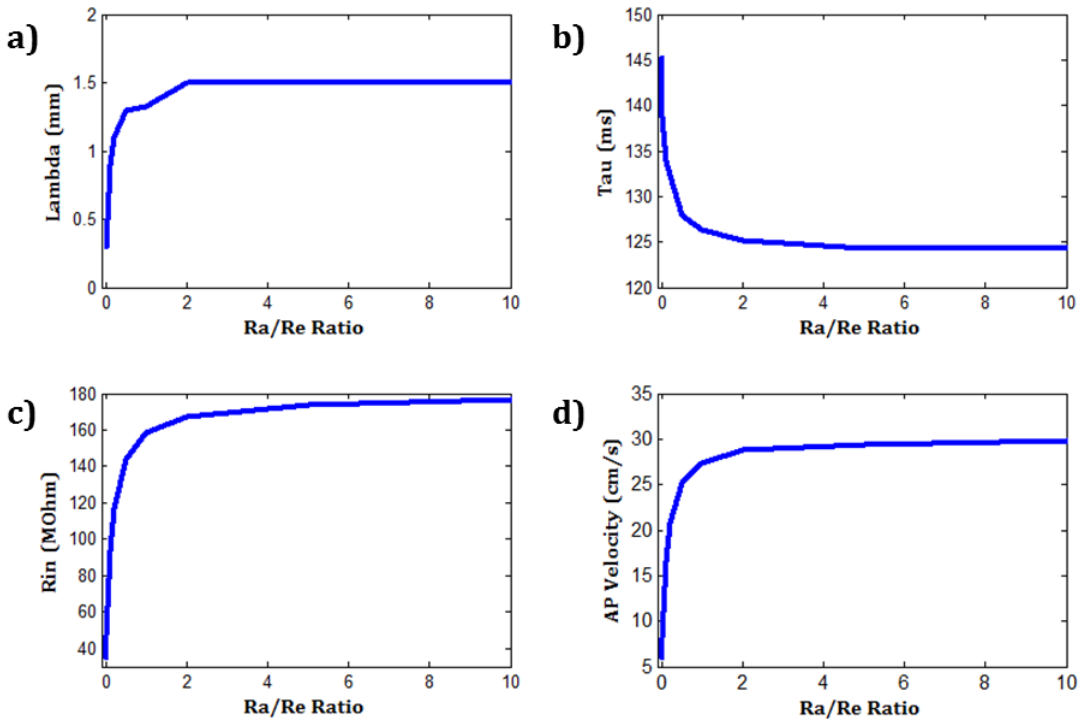

Figure 8: Variation in electrical properties determined for the central cell in a 1-D chain of cells, coupled both intracellularly and extracellularly, with changes in the ratio of intracellular to extracellular resistance. The panels show (a) the membrane length constant, (b) the membrane time constant, (c) the input resistance, and (d) AP conduction velocity.

3.3 Recording Extracellular Electrical Activity

Here we consider a 3-D syncytial model of size 5-cube (5 x 5 x 5 cells). The implementation of the continuous extracellular space allows us to obtain extracellular recordings during simulations. Fig. 9 shows simultaneous intracellular and extracellular recordings of a synaptic potential at the centroidal cell in the syncytium. It is seen that for Ra/Re = 4, the membrane potential depolarizes by around 3.5 mV, but the extracellular potential only varies by a maximum of 33 μV. If the volume of interstitial space is reduced by setting Ra/Re = 0.01 (as discussed in the following section), then the same stimulus produces a 12.7 mV depolarization and 10.5 mV extracellular

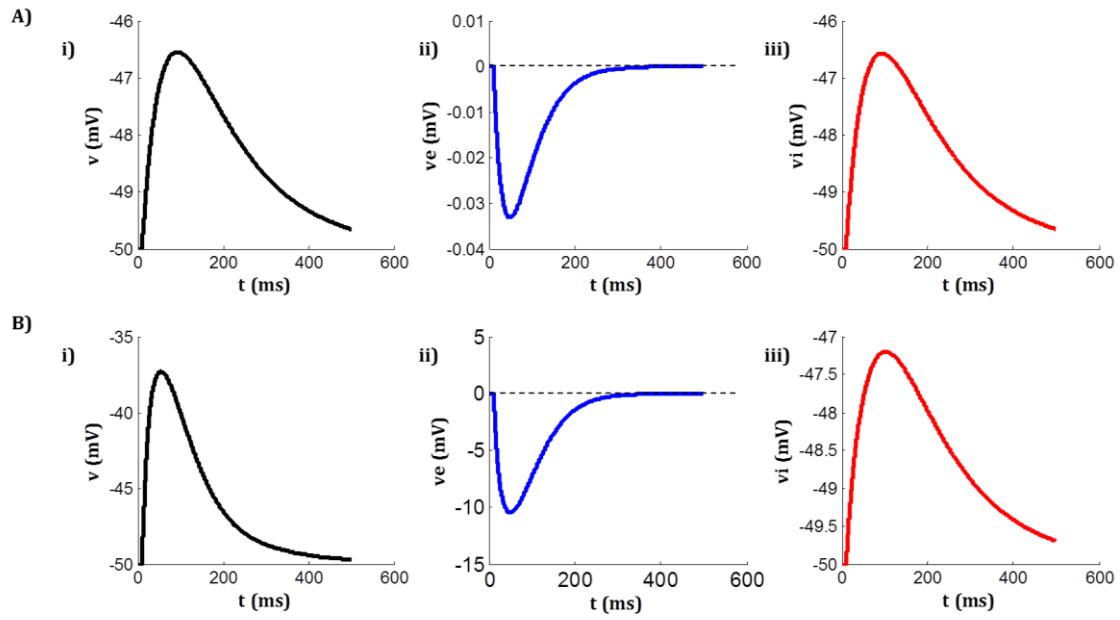

Figure 9: Simultaneous intracellular and extracellular recordings of synaptic potentials at the centroidal cell in a 3-D syncytial model of size 5-cube. Panels in A and B show recordings for Ra/Re = 4 and 0.01, respectively. Panels plot (i) transmembrane potential, (ii) extracellular potential, and (iii) intracellular potential. The extracellular potential peaks well before the intracellular potential. Note particularly the large change in extracellular potential on changing Ra/Re (see ranges of ordinate).

potential. In the latter case, the peak extracellular potential is even larger than the peak intracellular potential (10.5 mV vs 2.8 mV). It should be noted that the change in extracellular potential is negative-going, and opposite in polarity to the membrane potential.

Fig. 10 shows simultaneous intracellular and extracellular recordings from two different cells in our model. The trace in red is obtained from the centroidal cell, which is stimulated by means of supra-threshold synaptic input. The blue trace shows the propagated AP at a distant, non-peripheral cell in the syncytium. The extracellular recordings from these cells show that the extracellular AP has a biphasic shape at the site of stimulation, and as it propagates to other cells, it exhibits a triphasic extracellular AP, as expected from biophysical considerations (Stys & Kocsis, 1995). The first phase

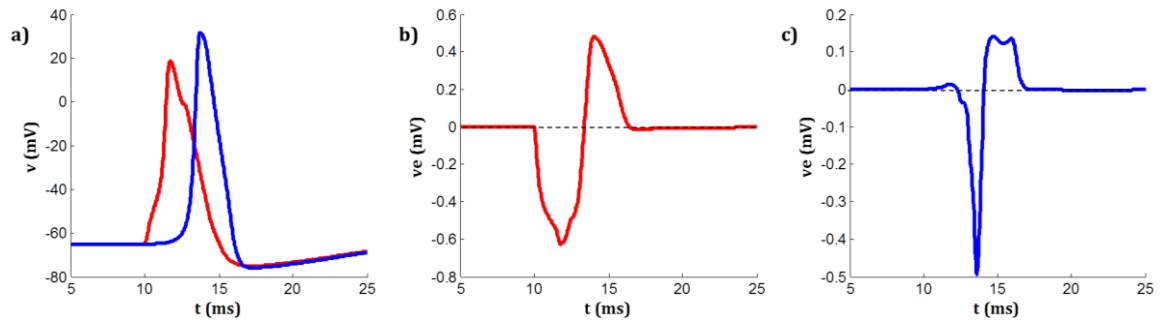

Figure 10: Simultaneous intracellular and extracellular recordings of APs at two different cells in a 3-D syncytial model of size 5-cube. Red trace in (a) shows the AP at the site of stimulus, while the blue trace shows propagated AP recorded at a distant cell. Panels (b) and (c) show the extracellular recordings of the APs at these cells.

(positive), corresponding to the AP foot, arises from local circuit currents, while the second phase (negative) is an outcome of the large rapid influx of Na^+ ions leading to the peak of the AP. The third phase (positive) corresponds to the repolarization phase of the AP involving efflux of K^+ ions (Sperelakis, 2012). At the site of stimulation, the AP is elicited not owing to local circuit currents (first phase above), but due to inward current from the synaptic input. This, in combination with the influx of Na^+ ions (second phase above), is recorded extracellularly as a single negative going potential, followed by the efflux of K^+ ions (third phase above), resulting in a biphasic waveform at the site of stimulation.

3.4 Exploring Ephaptic Coupling

To explore ephaptic coupling, we removed the gap junctions from our 3-D syncytium model having HH channels. The cells were now coupled merely by means of the continuous extracellular field. Supra-threshold stimulus, as before, was applied at the centroidal cell by means of synaptic input. In the absence of gap junctions, this elicited AP was unable to propagate to neighboring cells. Sub-threshold depolarizations could

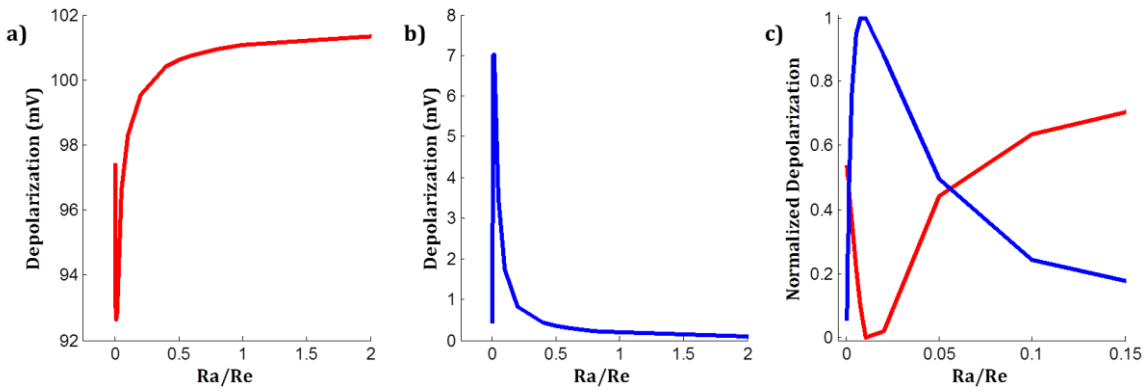

Figure 11: Peak depolarizations at (a) the centroidal cell, and (b) a neighboring cell, following stimulation via synaptic input at the centroid cell in a 3-D syncytial model of size 5-cube. Data in panel (a) corresponds to action potentials, whereas that in (b) corresponds to sub-threshold potentials. Cells are not coupled intracellularly, but linked extracellularly. (c) shows the peak depolarizations of the two cells, following min-max normalization of the plots in (a) and (b), for small values of Ra/Re.

be recorded at the immediately neighboring cells. We examined the peak depolarizations achieved at a neighboring cell with changes in Ra/Re. The results are summarized in Fig. 11. A non-monotonic trend was observed, with the transition occurring around Ra/Re = 0.01 for our model. The largest peak depolarization (7 mV) at the neighboring cell was recorded at this level. For ratios greater than 0.01, the peak depolarization at the centroid cell (AP height) gradually increased, whereas the peak sub-threshold depolarization in the neighboring cell correspondingly decreased. As in Fig. 8, it was found that the trends began to settle from Ra/Re = 2 onwards. Interestingly, for ratios smaller than 0.01, corresponding to progressively sparser interstitial space, the AP height at the centroidal cell was found to increase with a concomitant decrease in the peak depolarization at the neighboring cell.

The above simulations indicated that ephaptic coupling independently would be unable to elicit APs in our model. We thus decided to explore whether they could potentially play a contributory role, in combination with gap junctional coupling. The default value

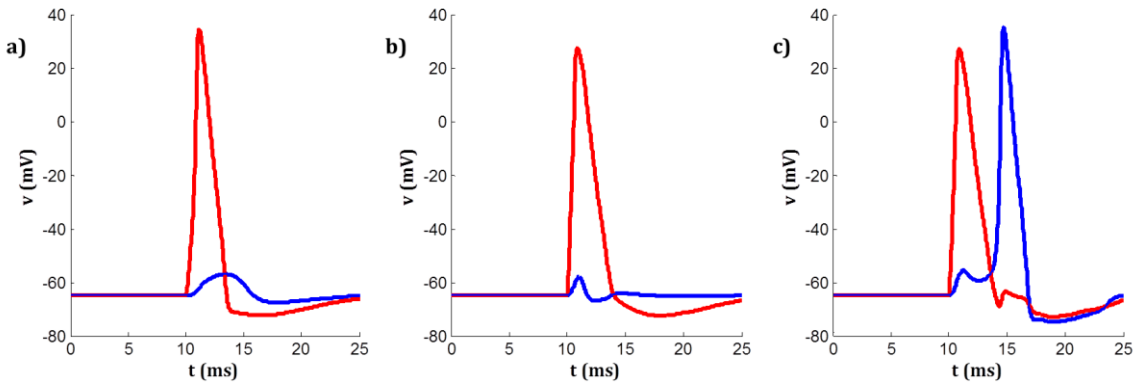

Figure 12: Response of centroidal cell (in red) and its immediate neighbor (in blue) in a 3-D syncytial model of size 5-cube. Stimulus was applied via synaptic input under (a) only gap junctional coupling, (b) only ephaptic coupling, (c) both gap junctional and ephaptic coupling

of gap junctional resistance (R_j) of 30.6 MΩ was known to elicit APs, even in the absence of ephaptic coupling (Appukuttan et al., 2015b). Therefore, we reduced the gap junctional coupling, by setting R_j = 330 MΩ, so that intercellular coupling by itself could not support propagating APs (Fig. 12a). The ratio Ra/Re was set to 0.01, corresponding to the largest peak depolarization in the neighboring cell, observed earlier. As seen in Fig. 12c, the combined effect of gap junctional and ephaptic coupling elicited APs in the neighboring cells, and these propagated through the entire syncytium.

3.5 A Toy Neuron Model

To demonstrate the generality of the technique presented here to couple extracellular fields of individual cells, we present, as an example, the implementation of the same to couple two neurons. The two neurons, as show in Fig. 13, have been considered to be identical and located in close spatial proximity, thereby introducing the possibility of ephaptic interactions. Each neuron consists of a soma, axon, and two proximal dendrites, each of which divides into two distal dendrites. The biophysical properties

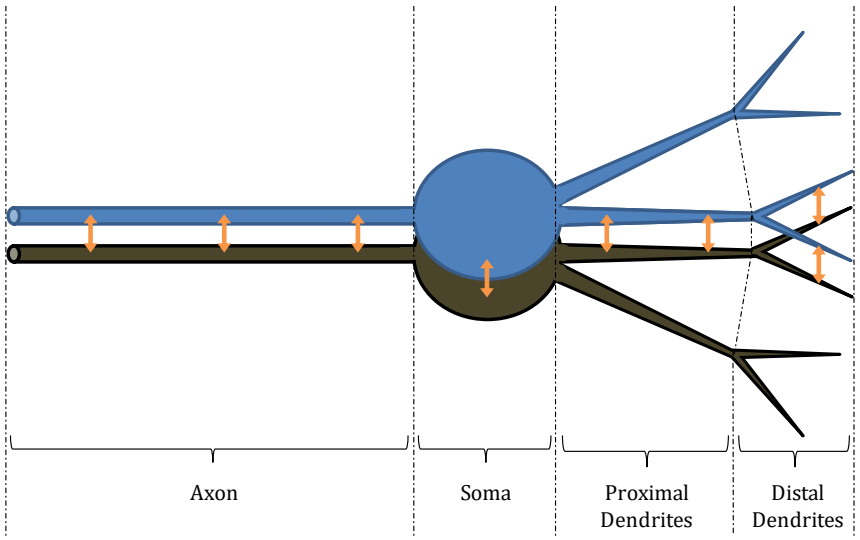

Figure 13: Two neurons positioned very close to each other. The arrows indicate sections where the extracellular fields of the two neurons are coupled. Only one of the primary dendrites, and its subtree, of each neuron is linked. This is to show that it is possible to restrict the coupling to only certain regions of the neuron.

used for developing the neuron model are presented in section S1.1 (supplementary document), along with the NEURON code for constructing the model in section S1.2. The neurons have been considered to be oriented such that one primary dendrite of each neuron, along with the distal dendrites emerging from it, is considered to be at a sufficiently large distance from the other neuron to not have their extracellular spaces affected directly by it. Such a constraint has been imposed to introduce an element of heterogeneity in the coupling of the extracellular regions of the two neurons, and to show that it is possible to restrict the coupling to only certain regions of the neuron. This can be made furthermore complex, if required, as discussed in section S1.3.

We performed some simulations using the dummy model to demonstrate its functionality. Fig. 14 shows results from a study to observe the ephaptic interactions between the two neurons. It was found that an AP elicited in one of the neurons, by means of current injection at the soma, is able to evoke an AP in the adjacent neuron only for a certain range of Ra/Re values. Fig. 15 provides a more detailed representation

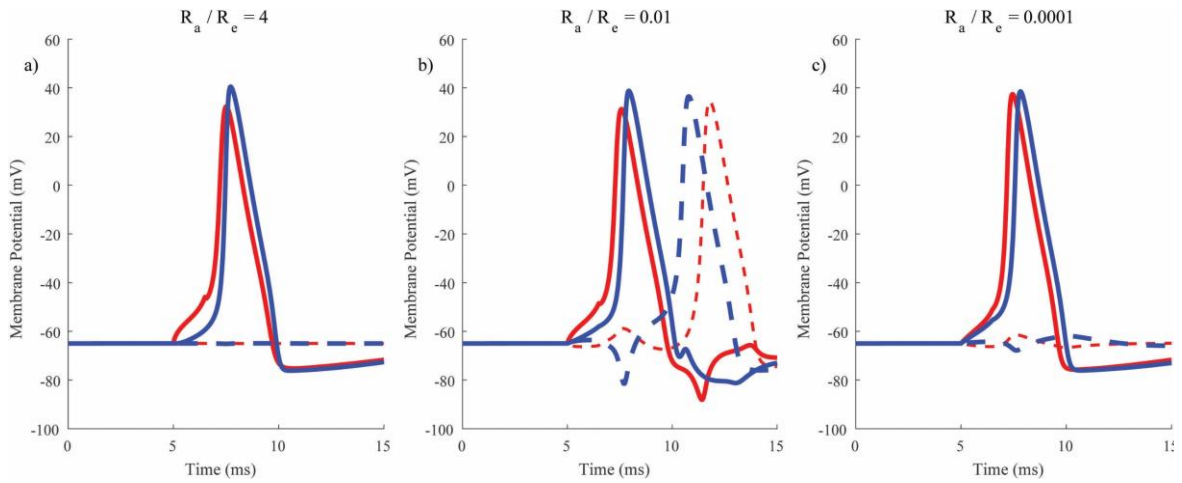

Figure 14: Electrical activity recorded at the soma (red) and axon (blue) of the two neurons for different Ra/Re values. The stimulated neuron is plotted with solid lines, while the other adjacent neuron is plotted with dashed lines.

of these test results. It shows the peak depolarizations attained by the non-stimulated neuron, following elicitation of AP at the soma of the other neuron. It can be observed that the non-stimulated neuron produces APs, at its soma and axon, only for a window of Ra/Re values. These results are essentially similar to those presented for the model of the smooth muscle syncytium presented in Fig. 11.

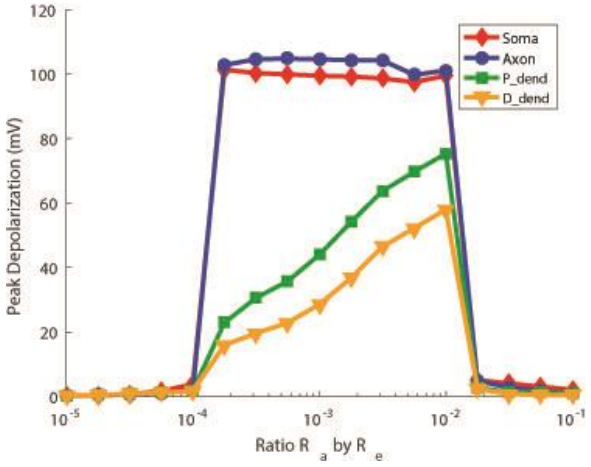

Figure 15: Peak depolarization attained at different regions of the non-stimulated neuron, when an AP is elicited in the stimulated neuron, for different values of Ra/Re. It is seen that that the stimulated neuron can evoke an AP in the adjacent neuron, via ephaptic interactions, only for a window of Ra/Re values.

4. Discussion

To our knowledge this is the first attempt to develop, on a compartmental modeling platform, a three-dimensional model of an electrical network of cells, where the cells are not just coupled intracellularly but extracellularly as well. The only other related modeling work in this domain is the NEURON implementation (ModelDB Accession: 3676; Michael Hines, Yale University) of the analytical model by Bokil et al. (2001), which is restricted to the demonstration of ephaptic interactions between a pair of axons. LFPy (Lindén et al., 2013) and LFPsim (Parasuram et al., 2016) are examples of other tools that address the issue of simulating extracellular fields. An important distinction between these and the present work, however, is that the former specifically target the recording of local field potentials as population signals. But no provision exists for the extracellular potentials so evaluated, to influence the intracellular potentials. This is a prerequisite for studying ephaptic interactions, where cells interact via extracellular potentials influencing their intracellular activity. In the present work, we have demonstrated the coupling of the extracellular field of every cell in a three-dimensional model to obtain a continuous uniform extracellular space, with each cell capable of contributing and being affected by the extracellular interactions.

Through the evaluation of passive and active electrical properties under various extents of intracellular to extracellular resistance, we were able to demonstrate that the electrical response of cells is influenced by the extracellular field. These effects are particularly notable when the extracellular space is limited. Observations such as the decrease in conduction velocity with a reduction in the extracellular volume are in accord with previously reported studies (Roth, 1991).

435 The extracellular amplitudes of synaptic potentials, under a relatively large volume of
436 extracellular space, were found to be on the order of μV. This is in agreement with
437 previous experimental findings (Manchanda, 1995). In electrophysiology, recordings
438 obtained using sharp microelectrodes usually measure the potential with respect to a
439 reference electrode connected to ground. The recorded potential would, technically, be
440 the intracellular potential, and not the true membrane potential. From Fig. 9, it can be
441 seen that there exists a notable difference between the intracellular potential and the
442 membrane potential when the extracellular space is constrained (Ra/Re = 0.01), but not
443 so prominent when there is a large volume of extracellular space (Ra/Re = 4). This
444 might have implications in the interpretation of electrophysiological data from tissues
445 having tightly packed cells, and a computational model, such as the one presented here,
446 could prove helpful in their analysis. Past studies have also shown that an AP, when
447 recorded extracellularly at the site of stimulation, would exhibit a biphasic waveform, while
448 those recorded distantly would be triphasic (Stys & Kocsis, 1995). We were able to confirm
449 these trends in simulations using our model (Fig. 10).

450 Our simulations exploring ephaptic coupling did not suggest a significant role for this
451 form of coupling in syncytial interactions when acting by itself. But it showed potential
452 to contribute towards AP propagation in poorly coupled networks of cells. This might be
453 significant in the context of poorly coupled syncytial tissues, such as the mouse detrusor
454 (Meng et al., 2008) or vas deferens (Holman et al., 1977). Our simulations also showed
455 that the model was capable of exhibiting extracellular potentials of the order of
456 millivolts for certain configurations of the extracellular space. This corresponds to the
457 findings by Goldwyn & Rinzel (2016) where they demonstrated that a neuronal
458 population could generate millivolt-scale extracellular potentials, and that this could
459 induce millivolt-scale perturbations in the membrane potential of a neuron. The present

study is preliminary, and a more focused investigation is required to be undertaken for physiologically relevant interpretations. Our model enables such a study to be performed, with possible enhancements including increased density of ionic channels at regions of overlap, and dynamic changes of ionic concentration in the interstitial space.

It is interesting to note that similar trends were observed for the syncytial smooth muscle model and the toy neuron model. Both models showed that the strength of ephaptic influences was significant only for a window of Ra/Re values, and diminished when the extracellular space was further limited. These models represent different cellular units and morphologies, and yet exhibit similar behavior.

The results presented here provide confidence in our implementation of a continuous extracellular space for a three-dimensional network of cells. This provides a framework for further investigation of interactions in tightly packed networks of cells, such as the interaction between nerve fibers and cells in an electrical syncytium.

Acknowledgments — The work was supported by grants from the Department of Biotechnology (DBT), India (BT/PR12973/MED/122/47/2016) and the UKIERI (UKUTP20110055). The authors would like to thank Michael Hines and Ted Carnevale (Yale University) for their continued expert technical support with NEURON.

References

Appukuttan, S., Brain, K. L. & Manchanda, R. (2015a). A computational model of urinary bladder smooth muscle syncytium. *Journal of computational neuroscience* **38** (1), 167--187.

Appukuttan, S., Brain, K. L. & Manchanda, R. (2015b). Syncytial Basis for Diversity in Spike Shapes and their Propagation in Detrusor Smooth Muscle. *Procedia Computer Science* **51**, 785--794.

Bédard, C., & Destexhe, A. (2013). Generalized cable theory for neurons in complex and heterogeneous media. *Physical Review E*, **88**(2), 022709.

Bennett, M., Gibson, W. & Poznanski, R. (1993). Extracellular current flow and potential during quantal transmission from varicosities in a smooth muscle syncytium. *Philosophical Transactions of the Royal Society of London. Series B: Biological Sciences* **342** (1300), 89--99.

Bokil, H., Laaris, N., Blinder, K., Ennis, M. & Keller, A. (2001). Ephaptic interactions in the mammalian olfactory system. *J Neurosci* **21**, 1--5.

Casaleggio, A., Hines, M. L. & Migliore, M. (2014). Computational model of erratic arrhythmias in a cardiac cell network: the role of gap junctions. *PloS one* **9** (6), e100288.

Crane, G. J., Hines, M. L. & Neild, T. O. (2001). Simulating the spread of membrane potential changes in arteriolar networks. *Microcirculation* **8** (1), 33--43.

Goldwyn, J. H., & Rinzel, J. (2016). Neuronal coupling by endogenous electric fields: cable theory and applications to coincidence detector neurons in the auditory brain stem. *Journal of Neurophysiology*, 115(4), 2033-2051.

Hines, M. & Carnevale, N. T. (2001). NEURON: a tool for neuroscientists. *The Neuroscientist* **7** (2), 123--135.

Hines, M. L. & Carnevale, N. T. (1997). The NEURON simulation environment. *Neural Computation* **9** (6), 1179--1209.

Holman, M. E., Taylor, G. & Tomita, T. (1977). Some properties of the smooth muscle of mouse vas deferens. *The Journal of physiology* **266** (3), 751.

Holt, G. R. & Koch, C. (1999). Extracellular interactions via the extracellular potential near cell bodies. *Journal of computational neuroscience*. 6, 169-184.

Jack, J. J., Noble, D. & Tsien, R. W. (1975). *Electric current flow in excitable cells.*

519 Clarendon Press (Oxford).
520
521 Keener, J. P. (1990). The Effects of Gap Junctions on Propagation in Myocardium: A
522 Modified Cable Theory. *Annals of the New York Academy of Sciences*, **591**(1), 257-277.
523
524 Keener, J. P. (1991). The effects of discrete gap junction coupling on propagation in
525 myocardium. *Journal of theoretical biology*, **148**(1), 49-82.
526
527 Koch, C. (2004). Biophysics of computation: information processing in single neurons.
528 Oxford university press.
529
530 Lin, J. & Keener, J. P. (2013). Ephaptic coupling in cardiac myocytes. *IEEE transactions on*
531 *bio-medical engineering* **60** (2), 576--582.
532
533 Lindén, H., Hagen, E., Łęski, S., Norheim, E. S., Pettersen, K. H., & Einevoll, G. T. (2013).
534 LFPy: a tool for biophysical simulation of extracellular potentials generated by detailed
535 model neurons. *Frontiers in Neuroinformatics*, 7.
536
537 Manchanda, R. (1995). Membrane Current and Potential Change During Neurotransmission
538 in Smooth Muscle. *Current Science* **69** (2), 140--150.
539
540 Meng, E., Young, J. S. & Brading, A. F. (2008). Spontaneous activity of mouse detrusor
541 smooth muscle and the effects of the urothelium. *Neurourology and Urodynamics* **27** (1), 79-
542 -87.
543
544 Migliore, M., Hines, M. L. & Shepherd, G. M. (2005). The role of distal dendritic gap
545 junctions in synchronization of mitral cell axonal output. *Journal of computational*
546 *neuroscience* **18** (2), 151--161.
547
548 Mori, Y., Fishman, G. I. & Peskin, C. S. (2008). Ephaptic conduction in a cardiac strand
549 model with 3D electrodiffusion. *Proc. Natl. Acad. Sci. U.S.A.* **105**, 6463-6468.
550
551 Parasuram, H., Nair, B., D'Angelo, E., Hines, M., Naldi, G., & Diwakar, S. (2016).
552 Computational modeling of single neuron extracellular electric potentials and network local

field potentials using lfpsim. *Frontiers in Computational Neuroscience*, 10.

Plonsey, R., & Barr, R. C. (1991). *Bioelectricity: a quantitative approach*. Plenum Press.

Rall, W. (1959). Branching dendritic trees and motoneuron membrane resistivity. *Experimental neurology*, 1(5), 491-527.

Rall, W. (1964). Theoretical significance of dendritic trees for neuronal input-output relations, in: Neural Theory and Modeling, R.F. Reiss, ed., Stanford University Press, Palo Alto, 73-97.

Roth, B. J. (1991). Action potential propagation in a thick strand of cardiac muscle. *Circulation research* **68** (1), 162--173.

Roth, B. J. (1997). Electrical conductivity values used with the bidomain model of cardiac tissue. *IEEE Transactions on Biomedical Engineering* **44** (4), 326--328.

Sperelakis, N. (2002). An electric field mechanism for transmission of excitation between myocardial cells. *Circulation research* **91** (11), 985--987.

Sperelakis, N. & McConnell, K. (2002). Electric field interactions between closely abutting excitable cells. *Engineering in Medicine and Biology Magazine, IEEE* **21** (1), 77--89.

Sperelakis, N. (2012). Cable properties and propagation of action potentials, in: Cell physiology source book: essentials of membrane biophysics, N. Sperelakis, ed., Elsevier, 395-416.

Stys, P. & Kocsis, J. (1995). Electrophysiological approaches to the study of axons. *The Axon: Structure, Function and Pathophysiology*, Oxford Univ. Press, New York., 328--340.

Suenson, N. (1991). Factors related to the propagation of the cardiac impulse: ephaptic impulse transmission and curved wavefronts of excitation, in: Intercellular Communication, F. Bukauskas, ed., Manchester University Press, pp. 223.